JOURNAL OF MATERIALS SCIENCE 19 (1984) 1897–1903

Subsurface imaging of glass fibres in a polycarbonate composite by acoustic microscopy

R. L. HOLLIS, R. HAMMER
IBM Thomas J. Watson Research Center, P.O. Box 218, Yorktown Heights, New York 10598, USA

M. Y. AL-JAROUDI
Material Analysis Laboratory, IBM Svenska Aktiebolag, Datavagen 11, S-175 87 Jarfalla, Sweden

Using reflection acoustic microscopy at 800 MHz, we have imaged 10 μm diameter glass fibres embedded in an optically opaque Makrolon™ (polycarbonate) matrix. Maximum depth of acoustic waves contributing to image formation was 105 μm, with imaging resolution of several microns at shallower depths. The areal fibre distribution, lengths, and orientations were readily determined non-destructively from the acoustic images. Additionally, marked differences were observed between known normally bonded samples with high strengths, and poorly bonded samples from parts which exhibited fracturing and premature failures. In addition to acoustic microscopy, bulk sound velocity measurements were made and used to compute focus aberration for subsurface imaging. Results were correlated with destructive SEM techniques.

1. Introduction

Often it is desirable to know the distribution, orientation, and adhesion properties of reinforcing fibres in composite materials. Except for fibres lying at the surface, few non-destructive analytical techniques are available to make these determinations. The usual procedure is to use fractographic analysis wherein the sample under investigation is sacrificed by fracturing with subsequent inspection by an optical or scanning electron microscope. A useful characteristic of the acoustic microscope is its ability to provide subsurface information non-destructively. A diffraction-limited acoustic beam is allowed to impinge on the sample and comes to focus at some depth beneath the surface. For most organic materials which generally exhibit low acoustic impedances, there is a good match between the material and the droplet of water used to transmit sound waves in the space between the lens and the sample surface giving good depth penetration. The incident sound pulses are reflected by subsurface features such as the glass fibre reinforcing elements and return to the surface where they are detected and imaged.

2. Makrolon™ plastic

The materials used in this study were planar specimens of reinforced and unreinforced Makrolon™ plastic* (polycarbonate), referred to in the remainder of this paper simply as polycarbonate. Polycarbonate is a rigid high-molecular-weight, low-crystalline thermoplastic material providing exceptional impact resistance since it yields in a ductile manner, rather than shattering. Unfilled polycarbonate begins to flow under stresses of the order of 60 MPa and reinforced types, depending on glass fibre content, fail immediately after exceeding the yield point of between 80 and 130 MPa.

Polycarbonate materials are in general not

*See, for example [1], and [2] for a brief description of Makrolon™, and [3] for more detailed information.

0022–2461/84 $03.00 + .12

affected by acids, oil or greases and are largely used for industrial applications in cars, electronics, computer terminals, safety helmets, food trays and many other items. Polycarbonate has high heat deflection temperature. The unfilled material does not deflect under its own weight up to 135° C while some reinforced types raise this temperature level up to 140 to 145° C. Water absorption is 0.17% by weight at room temperature and 60% r.h. Polycarbonate with 30% glass fibre (Makrolon™ 8030) has a density of 1.42 g cm^{-3} whereas the unfilled material is 1.2 g cm^{-3}.

The tensile properties of filled polycarbonate are deteriorated if the adhesion between the glass fibres and the plastic matrix is poor. The adhesion is affected by temperature, pressure, and surface treatment of the glass fibres. To aid in understanding differences that we had seen in initial acoustic micrographs of this material, sound velocity measurements of samples from fabricated parts with high strength, and from samples with low strength which exhibited premature failures, were obtained.

To measure sound velocity, a pulsed transmission technique was used in which time between an initial pulse and a transmitted pulse was measured [4]. A 15 μsec pulse at a 1 kHz repetition rate was used. Samples ranging in thickness from 3 to 6.7 mm were mounted between PZT transducers with grease used as a coupling agent. These measurements are summarized in Table 1. Samples exhibiting low strength had velocities approaching the unfilled material, whereas samples known to have high strength had considerably greater velocities as expected due to the higher sound velocity of the glass fibres.

TABLE I Bulk longitudinal sound velocities of polycarbonate samples used in this study

Sample No.	Glass content (%)	Velocity (m sec^{-1})	Comments
1	0	2000	Control (unfilled) test slab
2	30	3200	High strength test slab
3	30	2200	Low strength part
4	30	2300	Low strength test slab

3. Acoustic microscope

We have constructed a pulsed-reflection acoustic microscope following Lemons and Quate [5]. A thin-film ZnO transducer is used, which operates both as a transmitter and receiver. The transducer is grown on a sapphire rod whose *c*-axis is aligned with the acoustic beam. A 200 μm radius spherical cavity with quarter-wave matching layer forms the acoustic lens on the opposite end of the sapphire rod. Fig. 1 is a diagram of the transducer/lens assembly. Bursts of 800 MHz microwave energy are coupled into the transducer through a matching network. The piezoelectric transducer generates a plane longitudinal acoustic wave which propagates through the sapphire delay medium. The sapphire/water interface acts as a lens which brings the acoustic radiation to a sharp focus on the sample. Spherical aberration in this case is negligible because of the large difference in acoustic velocity between sapphire and water. However, additional aberration due to the sample

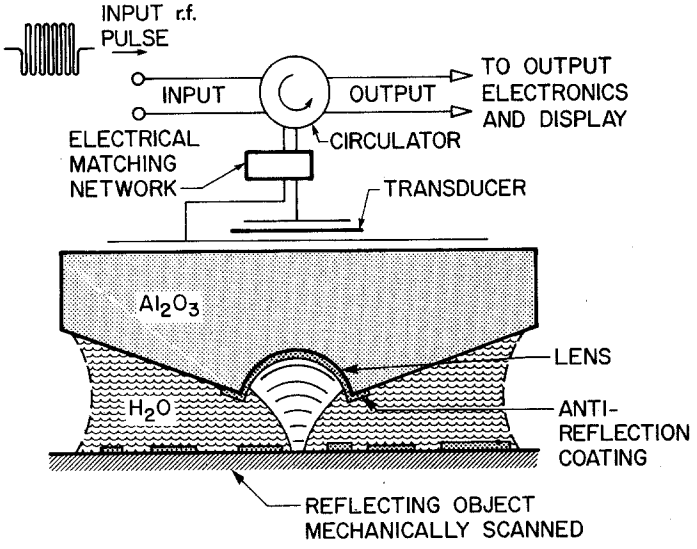

Figure 1 800 MHz acoustic lens and transducer. Input r.f. pulses are coupled to the transducer through a circulator and matching network. The ZnO transducer generates plane acoustic waves which propagate along the *c*-xis of the sapphire to the lens. Return signals are coupled out of the transducer and go to the amplifer electronics and display. r_0 = radius of lens = 200 μm. f = focal length of lens = $1.3r_0$. R = radius of lens aperture = $0.7r_0$ (from [5]).

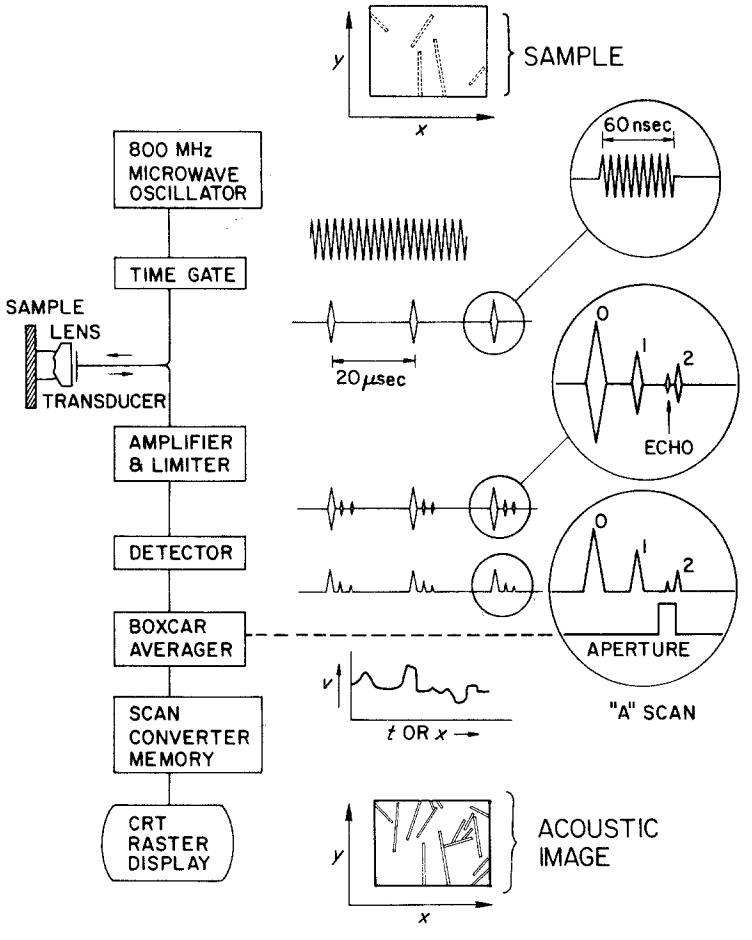

Figure 2 Schematic diagram of 800 MHz reflection acoustic microscope, showing typical signals. The sample is pulsed with 800 MHz focused acoustic waves while being mechanically scanned in x and y. The image is stored in an analog scan convertor memory before display on a CRT.

interface can be large. The phase and amplitude of the reflected acoustic wave depends on the elastic modulus, density, and viscosity of the sample surface and subsurface regions. The transducer integrates spatially over the returning non-planar wavefront to produce a voltage which is coupled out to the signal processing and display electronics. Operating at 800 MHz, we obtain a resolution at the surface of approximately 1.5 μm. Resolution beneath the surface is degraded due to aberration effects (cf. Section 4). Details of this arrangement have been reviewed elsewhere [6].

Fig. 2 is a schematic representation of our instrument, showing the principal electronic elements and signals. At the top of the figure is shown a typical sample, which in the present case is a planar surface of reinforced polycarbonate material. The corresponding acoustic image is shown at the bottom. To obtain the acoustic image, the sample is rapidly scanned in the x-direction while the acoustic lens is slowly translated in the y-direction to accomplish a raster scan. The scanning is done mechanically with voice coils using a digitally-commanded analog servo controlled by a small Z80-based microcomputer. Referring to Fig. 2, the 800 MHz microwaves are gated into 60 nsec bursts at a repetition rate of approximately 50 kHz. The return signal is amplified and limited, obtaining an output consisting of several pulses. The pulse labelled "0" is the direct r.f. leakage, whereas "1" and "2" are acoustic reflections from the lens surface. In the lens geometry employed, the signal from the sample arrives just before the second lens reflection. The pulse train is rectified by a diode and the pulse reflection of interest is gated out using a boxcar averager. The output of the boxcar is a voltage which varies as the sample is scanned. The scan convertor memory uses an electron beam to store this voltage signal as charge on an oxidized silicon target. The beam is scanned in exact synchronism with the mechanical scanning. After the scanning is completed (requiring perhaps 20 to 30 sec) the resulting charge pattern is read off at TV line rates and displayed

on a high-resolution CRT monitor. Hard-copy images are obtained by photographing the face of the CRT.

4. Subsurface imaging

In the usual case, reflection acoustic microscopy of materials such as metals or silicon includes a strong surface component due to the large difference in impedance between the liquid coupling agent (usually water) and the sample. For example, $Z_{Si}/Z_{water} = 13.3$. Also, acoustic rays entering the sample surface at angles with respect to the normal, are bent more steeply from the normal and come to indistinct focus at depths much shallower than the focal point in the liquid. Severe focal point aberration is introduced due to the sound velocity mismatch e.g. $v_{Si}/v_{water} = 5.7$.

Materials such as polycarbonate, on the other hand, which possess acoustic impedances and sound velocities which are much closer to water, allow good imaging of subsurface features, as demonstrated by our present results. From Table I, the measured longitudinal sound velocity in unfilled polycarbonate samples is approximately $2000\,\mathrm{m\,sec^{-1}}$. Density of the unfilled material is $1.2\,\mathrm{g\,cm^{-3}}$, giving an acoustic impedance $Z = \rho v = 2.4 \times 10^5\,\mathrm{g\,cm^{-2}\,sec^{-1}}$.

A ray diagram for subsurface imaging in polycarbonate is shown in Fig. 3. Rays with low angles of incidence θ focus at greater depths than do rays with large angles. This results in a focus aberration $A(\theta)$ which can be computed from the formula [7]:

$$A(\theta) = R\left[\frac{1}{1-C} - \left(\frac{\sin\theta}{\tan\phi} + 1 - \cos\theta\right)\right] + \left[Z\left(\frac{v_2}{v_3}\right)\left(1 - \frac{\cos\phi'}{\cos\phi}\right)\right], \quad (1)$$

where

$$C = \frac{v_2}{v_1}$$

$$\theta' = \sin^{-1}\left\{\frac{v_2}{v_1}\sin\theta\right\}$$

$$\phi = \theta - \theta'$$

$$\phi' = \sin^{-1}\left\{\frac{v_3}{v_2}\sin\phi\right\}$$

θ is the ray angle in the coupling medium measured from the lens axis, R is the radius of the lens, Z is the distance the sample has been displaced toward the lens ($Z = 0$ where the focal point of the lens is at the sample surface), v_1 is the longitudinal velocity in the sapphire lens material, v_2 is the velocity in the liquid propagating medium (water), and v_3 is the longitudinal or shear velocity in the sample (polycarbonate).

The first term in the expression is simply the (negligible) spherical aberration for the acoustic lens, whereas the second term represents the additional aberration due to refraction at the solid–liquid interface. Our lens has an opening half-angle of 50° giving a maximum incidence angle ϕ at the sample of 44°. Since the critical angle for total reflection is 48.6°, all the rays from the lens enter the sample. (For silicon, only a narrow cone of rays up to $\theta = 11°$ enter the surface.)

With our lens radius of $R = 200\,\mu\mathrm{m}$ and opening half-angle of 50°, the working distance is approximately $158\,\mu\mathrm{m}$. Translating the sample toward the lens by a practical distance of somewhat less than this amount, e.g. $140\,\mu\mathrm{m}$ as shown in Fig. 3, puts the paraxial focus at a depth of $105\,\mu\mathrm{m}$ below the surface of the polycarbonate sample. (We are concerned here only with trans-

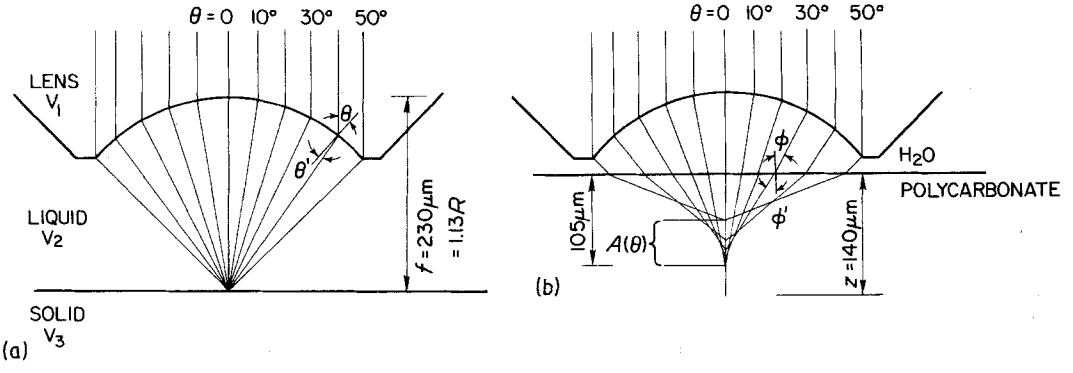

Figure 3 Ray diagram of acoustic lens imaging in polycarbonate material. (a) Focus at sample surface, (b) focus near maximum working distance.

mitted longitudinal waves. By applying acoustic boundary conditions at the liquid–solid interface we have calculated [8] that at the greatest incidence angle of 44°, 3% of the energy impinging on the surface is reflected, 30% is converted to shear waves and the remaining 67% to longitudinal waves.) Thus, for the samples with 10 μm diameter reinforcing fibres, we expect a maximum penetration depth of some 10 fibre diameters.

Evaluating Equation 1, the maximum total aberration of the outermost ray at a depth of $Z = 140\,\mu$m is approximately 51 μm. This defocusing is large when compared with the diffraction limit (approximately 2 μm lateral resolution in polycarbonate). However, some apodization of the lens is present, which decreases the contribution to the image from the larger angles. The total aberration appears small enough to allow good subsurface imaging in the present case.

5. Results

Images were obtained by acoustic and optical microscopy of unprepared samples, and SEM images of fractured samples. Strikingly different acoustic images were observed for low and high strength samples. Polycarbonate materials have no intrinsic colouring; however, all the specimens investigated were pigmented and therefore opaque so that only surface features were seen when viewed optically. However, when observed acoustically they appear highly transparent, as discussed in Section 3. For example, shown in Fig. 4 are optical and acoustic images of a specimen obtained from a low strength part which exhibited premature failure. Most prominent optically (Fig. 4a) are surface features and a few shallow, barely visible fibres. Images obtained acoustically, when focussed on the surface, are very similar (Fig. 4b), again with surface topographic features very apparent as well as the shallow subsurface fibres. However, shown in Fig. 4c, acoustic images taken with the lens moved toward the sample $Z = 24\,\mu$m clearly show many of the 10 μm diameter glass fibres to a depth of a few diameters, which are totally absent in the previous optical images, as well as those near the surface which scatter significant radiation back to the detector.

The difference between such a low strength specimen and one with high strength can be seen by comparison with Fig. 5. Whereas in the previous case many fibres were seen at a lower focal position, in the high strength case very few fibres are seen at any focal position. Shown in Fig. 5b is an image obtained at $Z = 15\,\mu$m. Here the same fibres are seen as in Fig. 5a but different portions of the fibres are in focus as expected at the lower focal position. Also, it should be noted that in the optical case, images of both samples are nearly identical, with only surface features showing, making it impossible to assess the degree of adhesion in that manner. The bright spots in the acoustic images are believed due to scattering from numerous small voids in the material.

One further difference between images of low and high strength can be seen in the images of Fig. 6. For low strength samples the sub-surface fibres appear to have considerably larger diameter (see Fig. 6a) then those few that are seen in high strength specimens (Fig. 6b). (Both images are at the same magnification.) This is due to the presence of cylindrical voids surrounding the fibres.

To further understand and to confirm these results, samples were sacrificed by fracturing and

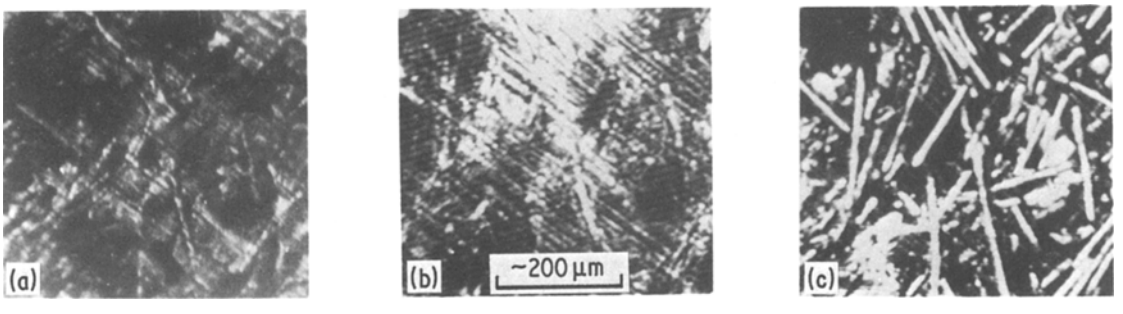

Figure 4 (a) Optical micrograph of polycarbonate composite surface. Note surface features and very few fibres. (b) Acoustic micrograph of the same region taken with the lens focused at sample surface. The resulting image resembles its optical counterpart. (c) Acoustic micrograph with lens at $Z = 24\,\mu$m, with many glass fibres visible at this focal plane which are undetected optically.

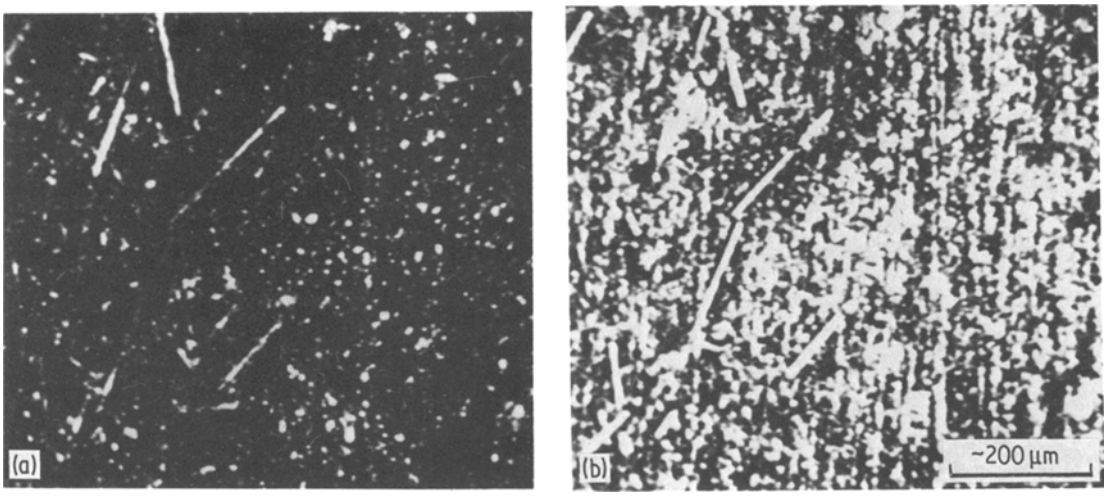

Figure 5 Acoustic micrograph of well-bonded polycarbonate composite at two different focal positions. (a) Near surface, (b) 15 μm below (a). Note the few sloping fibres observable in this well-bonded sample.

then inspected with a scanning electron microscope (SEM). The resulting images again showed marked differences between specimens of samples from fabricated parts with high strength, and low strength samples which exhibited premature failures. From these images the origin of the acoustic differences could be understood. As an example, Fig. 7a is an SEM image of a low strength sample which exhibited premature failure. An open matrix with poor adhesion to glass fibres resulting in cylindrical voids around many of the fibres can be seen. Acoustically these voids result in an impedance ratio mismatch (greater than 3.5×10^4 for glass/air compared to 6×10^0 for glass/polycarbonate). By comparison, the image in Fig. 7b of a well-bonded sample with high strength shows a much denser matrix and the absence of cylindrical voids. The large diameter voids of Fig. 7a cause the apparent larger fibre diameters seen in the acoustic micrographs of low strength specimens.

6. Conclusions

The subsurface fibres seen in acoustic micrographs are a direct result of cylindrical voids around poorly bonded fibres. Whereas the acoustic impedance of glass compared to polycarbonate is fairly close, the large difference between glass and the surrounding voids cause strong reflections that give

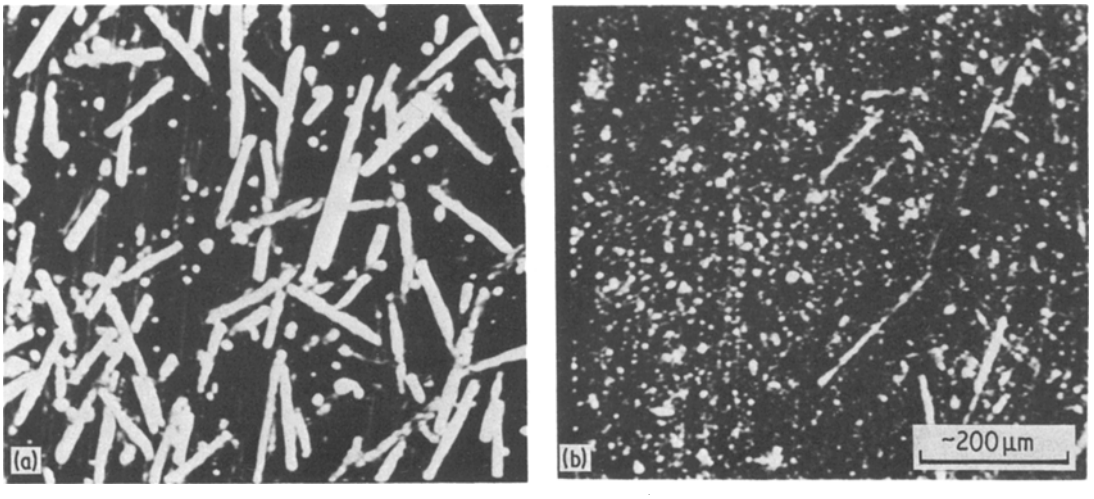

Figure 6 Comparison of specimens obtained with lens at $Z = 15$ μm to show subsurface fibres. (a) Low strength sample, (b) high strength sample.

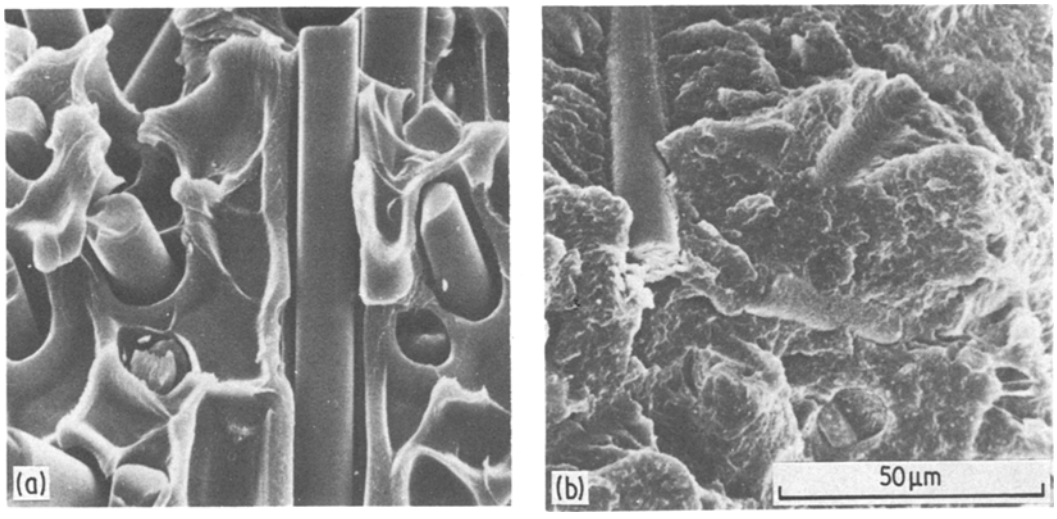

Figure 7 SEM micrographs of fractured surfaces; (a) poorly bonded polycarbonate composite, showing cylindrical voids around fibres, (b) same as (a) but fibres well bonded to the surrounding material and dense matrix.

rise to contrast in the acoustic images. High quality acoustic images of poorly adhered glass fibres in as-received samples can be obtained non-destructively and without the need for sample preparation. In addition, distributions, lengths and orientations of fibres are easily obtainable from these images. This information can be of great practical benefit in assessing, for example, fibre starvation in mould corners, etc.

The acoustic microscope appears presently to be the only instrument which can be used for non-destructive sub-surface imaging of composite materials like glass-fibre filled polycarbonate.

Acknowledgements

We thank C. E. Yeack for help with the sound velocity measurements, V. B. Jipson for helpful discussion, and E. J. Yarmchuk for help in boundary condition calculations.

References

1. C. A. HARPER, (ed.), "Handbook of Plastics and Elastomers" (McGraw-Hill, New York, 1975).
2. W. S. MILLER, (ed.), *Machine Design* **55** (1983) 166.
3. Bayer report E55-756-65943, edition KL40950, August, 1975.
4. J. E. ZIMMER and J. R. COST, *J. Acoust. Soc. Amer.* **47** (1969) 795.
5. R. A. LEMONS and C. F. QUATE, in 1973 Ultrasonics Symposium proceedings, IEEE cat. no. 73 (IEEE, New York, 1974) pp. 18–21.
6. R. L. HOLLIS and R. HAMMER, in "Scanned Image Microscopy", edited by E. A. Ash (Academic Press, New York, 1980) pp. 155–64.
7. V. B. JIPSON, *Appl. Phys. Lett.* **35** (1979) 385.
8. L. M. BREKHOVSKIKH, "Waves in Layered Media" (Academic Press, New York, 1970) pp. 15–36.

Received 31 May
and accepted 21 September 1983